Design of the double-layer spray greenhouse spray system and its cooling effects

Jihang Xu[1,2,3,4,5†], Weizhen Sun[6†], Jian Wang[1,2,3,4,5], Sheng Shu[1,2,3,4,5], Zhanming Tan[1,3*]

(1. *Xinjiang Production & Construction Corps Key Laboratory of Facility Agriculture/College of Horticulture and Forestry, Tarim University, Alar 843300, Xinjiang, China*;
2. *College of Horticulture, Nanjing Agricultural University, Nanjing 210095, China*;
3. *A Key Laboratory of Horticultural Plant Biology, Ministry of Education/College of Horticulture and Forestry Sciences, Huazhong Agricultural University, Wuhan 430070, China*;
4. *Facility Horticulture Research Institute of Suqian, Suqian 223800, Jiangsu, China*;
5. *Sanya Institute of Nanjing Agricultural University, Sanya 572024, Hainan, China*;
6. *Beijing Kingpeng International Hi-Tech Corporation, Beijing 100094, China*)

Abstract: The existing plastic greenhouses in the Yangtze River Basin experience high temperatures in summer and low temperatures in winter, significantly impacting year-round greenhouse production. Double-layer plastic film greenhouses possess excellent thermal insulation in winter but suffer from high temperatures in summer. Spray cooling is an effective method for reducing summer temperatures in greenhouses, yet direct spraying increases the indoor humidity, which is detrimental to crop growth. To address these problems, the research team designed a double-layer spray greenhouse in which a spray system composed of nozzles was placed between the two layers of plastic films. This paper simulated the indoor temperature field of a greenhouse under different nozzle layouts using Computational Fluid Dynamics (CFD) software to identify the optimal spray system. Based on this analysis, the practical effectiveness of a double-layer spray greenhouse was examined, thereby providing theoretical justification for its promotion and application. The key findings are as follows: 1) When the nozzle spacing was 0.8 m, the nozzle was placed 0.2 m from the inner arch top, and the nozzle sprayed downwards, the average temperature inside the greenhouse was the lowest, representing the optimal nozzle layout. 2) Compared to a single-layer multispan greenhouse, the double-layer spray greenhouse had a higher average indoor temperature of 1.18°C in spring, with a lower average indoor temperature of 2.14°C in summer. The growth, yield, and fruit quality (soluble solids content, vitamin C content, and soluble sugar content) of tomatoes in the double-layer spray greenhouse were superior to those in the single-layer multispan greenhouse.

Keywords: greenhouse, spray system, CFD, nozzle layout
DOI: 10.25165/j.ijabe.20251805.9483

Citation: Xu J H, Sun W Z, Wang J, Shu S, Tan Z M. Design of the double-layer spray greenhouse spray system and its cooling effects. Int J Agric & Biol Eng, 2025; 18(5): 76–89.

1 Introduction

Temperature is the main factor restricting the yield and quality of horticultural plants. In recent years, facility horticulture has developed rapidly, making the high-temperature hazards in greenhouses increasingly prominent in many regions of China during the transition from spring to summer. Summer solar radiation causes a significant increase in the internal temperature of greenhouses, even exceeding the maximum temperature that crops can tolerate, which has an adverse effect on their quality and yield. Effective cooling measures need to be taken to achieve facility production. Tawalbeh et al[1] classified greenhouse cooling technologies into two major categories: passive cooling and active cooling. Passive cooling mainly relies on natural conditions and the design of greenhouse structures, such as natural ventilation and shading for cooling. Active cooling requires external energy input to achieve indoor temperature reduction, mainly including spray systems, wet curtain-fan systems, etc. Natural ventilation cooling is the most commonly used cooling measure in greenhouses. It can effectively regulate the indoor temperature and humidity, but its efficiency is affected by various factors such as the number and size of greenhouse openings and others[2]. The wet curtain-fan system accelerates the vaporization process of water mist in the wet curtain through forced ventilation. The vaporization of water mist absorbs heat and takes away the heat of the air, achieving the cooling of the air inside the greenhouse. The spray system sprays water mist into the greenhouse through nozzles, using the heat absorbed by the evaporation of the water mist to lower the indoor temperature. The research found that the atomization system can not only significantly reduce the internal temperature of the greenhouse, but also help to lower the temperature of the crops and the saturation pressure difference of water vapor in the outdoor air[3-5].

In practical applications, various cooling technologies exhibit distinct application characteristics and applicable scopes due to the differences in their cooling principles. However, all these

Received date: 2024-11-02 **Accepted date:** 2025-06-22
Biographies: **Jihang Xu**, MS, research interest: protected horticulture engineering, Email: 2021104121@stu.njau.edu.cn; **Weizhen Sun**, Assistant Engineer, research interest: facility agricultural science and engineering, Email: anthonyanna@126.com; **Jian Wang**, Associate Professor, research interest: protected horticulture engineering, Email: wangjian@njau.edu.cn; **Sheng Shu**, Professor, research interest: protected cultivation, Email: shusheng@njau.edu.cn.
†These authors contributed equally to this work.
***Corresponding author: Zhanming Tan**, Associate Professor, research interest: protected cultivation, Xinjiang Production & Construction Corps Key Laboratory of Facility Agriculture/College of Horticulture and Forestry, Tarim University, Alar 843300, Xinjiang, China，Tel: 15909976635, Email: tlmdxtzm@taru.edu.cn.

technologies have certain limitations and flaws. Relying solely on a single cooling technology makes it difficult to achieve the desired cooling effect and cannot meet all the requirements for greenhouse operation. Therefore, it is usually necessary to comprehensively apply multiple cooling technical means to achieve a better cooling effect[6]. With the development of modern agriculture, higher requirements have been put forward for the accuracy and efficiency of greenhouse environment regulation. CFD can be used to simulate fluid flow, heat transfer, mass transfer, and phase change, describing the temperature field distribution within greenhouses. It is an essential tool for greenhouse design and optimization[7-8]. Both Hu[9]and Ghoulem[10] validated the feasibility of the CFD method and used it to simulate spray cooling effects. In this study, CFD was used to simulate the indoor temperature field of a greenhouse under different nozzle layout schemes, resulting in an optimized spray system.

To address the issues of high summer temperatures and low winter temperatures in existing plastic greenhouses in the Yangtze River Basin of China, our research team previously designed a double-layer spray greenhouse. This design employs a double-layer plastic film structure to enhance insulation in winter and introduces a spray cooling system between the double arches to address the high temperatures in summer[11]. This spray cooling system achieves more uniform and efficient evaporative cooling by regulating the droplet size, spatial distribution, and spray angle, combined with the characteristics of the air flow organization inside the greenhouse. Compared with traditional methods, this system can significantly improve the cooling efficiency under the premise of low water consumption, while reducing the leaf surface wetting time and lowering the probability of disease occurrence. In addition, this study also conducted an in-depth analysis of the coupling mechanism between different spray modes (upward/downward) and the airflow field through a combination of experiments and simulations, providing a theoretical basis and technical support for the optimal design of the greenhouse spray cooling system. This research not only makes up for the deficiencies of the existing spray cooling technology in mechanism analysis and model construction, but also lays an important foundation for the development of future intelligent greenhouse environmental control systems.

2 Materials and methods

2.1 Double-layer spray greenhouse

The double-layer spray greenhouse is located in the Baima Teaching Base of Nanjing Agricultural University in Lishui District, Nanjing City (31°37′N, 119°10′E). This greenhouse runs north to south, with a length of 4 meters and a span of 12 meters (consisting of three spans, each 4 meters wide), covering an area of 48 square meters. Each span features a double-layer circular arched roof, with an outer roof shoulder height of 1.6 m and a peak height of 2.4 m, while the inner roof has a shoulder height of 1.2 m and a peak height of 2.0 m. Inside the double-layer greenhouse, an inner gutter is installed with a one-way slope of 2.5‰. The entire greenhouse is covered with PEP anti-dripping film. Inside the greenhouse, 120° dual-spray nozzles (nozzle diameter of 0.3 mm) are used, with a nozzle spacing of 1 meter. The nozzles are installed in an upward spraying configuration, as shown in Figure 1. The water for spraying is pressurized using a booster pump. The nozzle layout is depicted in Figure 2.

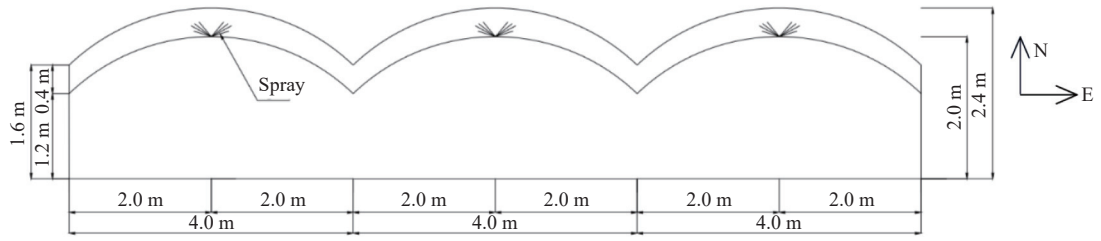

Figure 1 Schematic diagram of the double-spray greenhouse structure

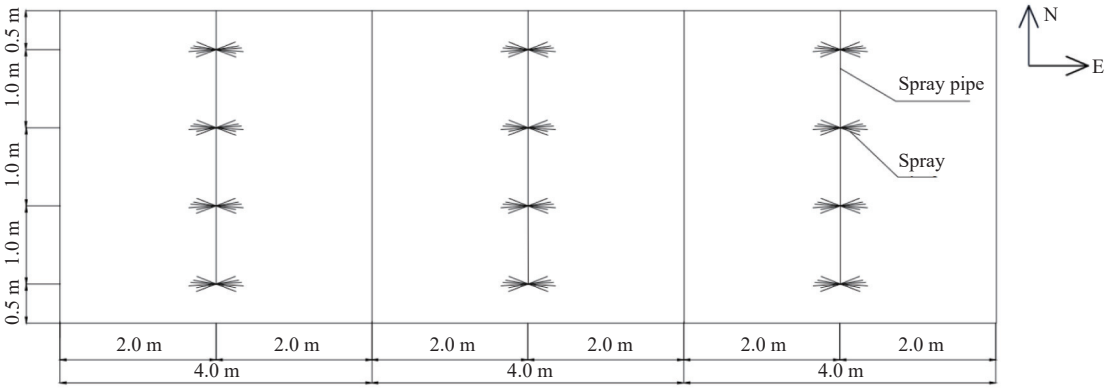

Figure 2 Schematic diagram of the nozzle layout

2.2 CFD numerical simulation

2.2.1 Basic governing equations

This study utilizes CFD software (Fluent 2021 R1) to conduct three-dimensional transient simulations of airflow within the greenhouse. The fluid dynamics within the greenhouse must satisfy the continuity equation, momentum equation, and energy equation, which can be expressed through flux equations as follows:

$$\frac{\partial(\rho\psi)}{\partial t}+\mathrm{div}(\rho\psi v^{v})=\mathrm{div}(\Gamma_{\psi}\mathrm{grad}\psi)+S'_{\psi} \quad (1)$$

where, ψ represents a general variable, such as u, w, v, or T. ρ represents density, kg/m^3; v^{v} represents the velocity vector, m/s; Γ_{ψ}

represents the generalized diffusion coefficient, and s_ψ represents the source term.

2.2.2 Turbulence modeling

In nature, common flows can be classified into turbulent and laminar flows. During the spraying experiment, the water mist and air continuously flow within the greenhouse, and the airflow is turbulent. The quality of the simulation results primarily depends on the choice of turbulence model, making it crucial to select the correct model. The standard k-ε model proposed by Launder and Spalding[12] is widely used, but it can yield large errors in calculating some nonuniform turbulent flow problems. Therefore, the realizable k-ε model is recommended, along with the enhanced wall treatment. The mathematical formula for this model is expressed as follows:

$$\frac{\partial}{\partial t}(\rho k)+\frac{\partial y}{\partial x}\left(\rho k u_j\right)=\frac{\partial}{\partial x_i}\left[\left(\mu+\frac{\mu_t}{\sigma_k}\right)\frac{\partial k}{\partial x_j}\right]+G_k+G_b-\rho\varepsilon-Y_M+S_k \tag{2}$$

$$\frac{\partial y}{\partial t}(\rho\varepsilon)+\frac{\partial}{\partial x_j}\left(\rho\varepsilon u_j\right)=\frac{\partial}{\partial x_j}\left[\left(\mu+\frac{\mu_t}{\sigma_\varepsilon}\right)\frac{\partial\varepsilon}{\partial x_j}\right]+\rho C_1 S_\varepsilon-\rho C_2\frac{\varepsilon^2}{k+\sqrt{v\varepsilon}}+C_{1\varepsilon}\frac{\varepsilon}{k}C_{3\varepsilon}G_b+S_\varepsilon \tag{3}$$

where, k represents turbulent kinetic energy, m^2/s^2; ε stands for turbulent dissipation rate, m^2/s^3; G_k represents the turbulent kinetic energy produced by the velocity gradient of laminar flow, m^2/s^3; G_b represents the turbulent kinetic energy generated by buoyancy, m^2/s^3; Y_M represents the fluctuation due to transitional diffusion in compressible turbulence, m^2/s^3; C_2 and $C_{1\varepsilon}$ are constants, σ_k and σ_ε are the turbulent Prandtl numbers for the k-equation and e-equation, respectively, and S_k and S_ε are user-defined terms, m^2/s^3.

2.2.3 Solar radiation model

Solar radiation is the energy source that shapes the temperature and humidity conditions inside a greenhouse and is an important parameter that affects the internal environment. When solar rays strike a plastic film greenhouse, part of the radiation is absorbed and reflected by its surface, while the remaining portion enters the greenhouse. Inside the greenhouse, some of the solar radiation is absorbed by the indoor air medium, while the rest is absorbed by the surrounding solid surfaces and the ground. Therefore, a solar radiation model must be incorporated during the simulation process. The discrete ordinates (DO) radiation model considers radiative heat transfer between gases and particles, allows radiation within semitransparent media, and does not require a specific optical thickness. As a result, this experiment utilizes the DO model to solve for radiative heat transfer within the greenhouse. This model treats the radiation equation propagating along the vector $\vec{s}$ as a specific field equation, and the specific equation is as follows:

$$\nabla\cdot(I(\vec{r},\vec{s})\vec{s})+(a+\sigma_s)I(\vec{r},\vec{s})=an^2\frac{\sigma T^4}{4\pi}+\frac{\sigma_s}{4\pi}\int_0^{4x}I(\vec{r},\vec{s})\Phi(\vec{S},\vec{S}')\mathrm{d}\Omega' \tag{4}$$

where, $\vec{r}$ represents the position vector; $\vec{s}$ represents the direction vector; $\vec{s}'$ represents the scattering direction vector; a represents the absorption coefficient; n represents the refractive index; σ_s represents the scattering coefficient; σ is the constant value of 5.627×10^{-8} W/(m^2·K^4); I represents the radiative intensity; T is the local temperature, K; Φ represents the phase function; Ω' represents the solid angle of space.

2.2.4 Porous media model

This experiment uses the porous media model to depict indoor crops. A three-dimensional mathematical model is established between the crop layer and the indoor gas flow velocity, and this model is subsequently included as a source term in the kinetic energy equation.

$$S_\varphi=-\left(\frac{\mu}{K_p}u+\frac{C_F}{\sqrt{K_p}}\rho u^2\right) \tag{5}$$

where, S_Φ represents the momentum source term, u represents the air velocity, kg/(m·s), C_F represents the nonlinear momentum loss factor, and K_P represents the permeability of the porous media.

2.2.5 Discrete phase model

The discrete phase model (DPM) can simulate the movement, evaporation, and heat exchange processes of spray droplets within the air inside a greenhouse. Based on the Euler–Lagrange method, this model treats the fluid as a continuous medium and the droplets as a discrete phase. The DPM follows Newton's second law of motion for the forces acting on particles in the flow field. Fluent predicts the trajectory of discrete phase particles (droplets) by integrating the forces acting on them, and this force balance is described in the Lagrangian coordinate system. The force balance equation can be written as Hu et al.[9]:

$$m_p\frac{\mathrm{d}\vec{u}_p}{\mathrm{d}t}=m_p\frac{\vec{u}-\vec{u}_p}{\tau_r}+m_p\frac{\vec{g}(\rho_p-\rho)}{\rho_p}+\vec{F} \tag{6}$$

where, m_p represents the mass of the particle, kg; $\vec{u}$ represents the velocity of the continuous phase, m/s; $\vec{u}_p$ represents the particle velocity, m/s, which represents the density of the continuous phase; ρ_p represents the density of the particle, kg/m^3; $\vec{F}$ represents the additional forces, m/s^2; and τ_r represents the relaxation time of the particle, s.

2.2.6 Boundary conditions

The greenhouse simulation system consists of four parts: the greenhouse envelope structure, soil, air, and water mist. The thermophysical property parameters are listed in Table 1. Based on the actual measured data at 15:00 on June 9, 2023, the indoor temperature was 43.50°C, and the relative humidity was 28.00%. The boundary types of the envelope structure, top, and ground of the greenhouse were set as walls, and the heat transfer mode was set as mixed heat transfer (including convective heat transfer and radiative heat transfer). The inner film of the double-layer greenhouse was set as the interior, the discrete phase boundary condition of the upper wall of the greenhouse was set as the wall-film, and the lower wall was set as the escape. The specific parameter settings are listed in Table 2. The spray characteristics and weather conditions on test days are listed in Tables 3 and 4.

Table 1 Thermophysical properties of different materials

Materials	Density/ kg·m^{-3}	Specific heat capacity/ J·kg^{-1}·K^{-1}	Heat conductivity/ W·m^{-1}·K^{-1}
Air	1.225	1006.43	0.0242
Plastic	923.000	2550.00	0.2900
Soil	1600.000	2200.00	0.8000
Water	998.200	4182.00	0.6000

Table 2 Boundary conditions

Parameters	Top surrounding enclosure	Ground
Heat condition	mixed	mixed
Heat transfer coefficient	6.60	2.94
Free stream temperature/°C	34.5	34.5
Material name	plastic	soil
Transparent type	semitransparent	opaque
External radiation temperature	1	1
Thickness/mm	0.15	100.00

Table 3 Settings of spray characteristics

Parameters	Temperature/°C	Atomization angle/(°)	Nozzle diameter/mm	Spray flow/kg·s^{-1}
Numerical value	26.85	62.85	0.30	0.0034

Table 4 Weather conditions on test days

Date	Weather conditions	Outdoor air temperature/°C	Maximum wind speed/m·s^{-1}	Maximum solar radiation value/W·m^{-2}
2023/6/9	Sunny	26-41	2.5	160

2.2.7 Initial conditions

The simulation was carried out under the condition of a typical sunny day (June 9, 2023 at 15:00), and the external climate conditions are listed in Table 4.

2.2.8 CFD simulation plan for nozzle layout

This experiment involved three different spraying heights, 0 m, 0.2 m, and 0.4 m from the top of the inner arch; three nozzle spacings, 0.8 m, 1.0 m, and 1.2 m; and two spraying patterns, upwards spraying and downwards spraying. The nozzle arrangement (taking the west span of the double-layer spraying greenhouse as an example, with the middle and east spans maintaining the same nozzle arrangement as the west span) is shown in Figure 3. A total of 12 simulation scenarios were summarized, as presented in Table 5.

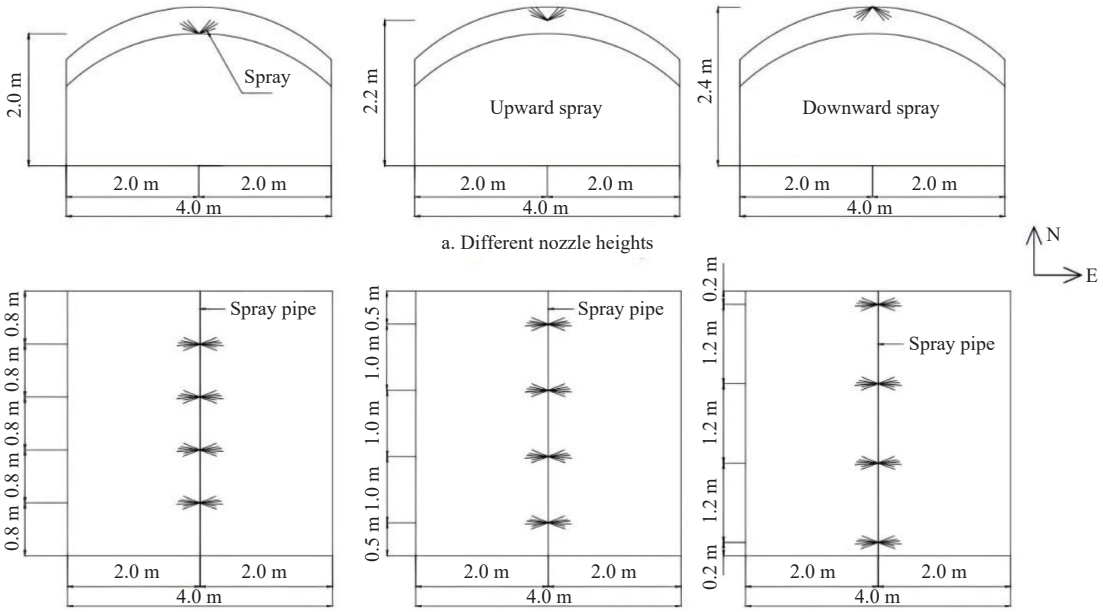

Figure 3 Schematic diagram of different nozzle heights and nozzle spacing

Table 5 Simulation scenarios

Options	Distance between nozzle and inner vault/m	Spacing of nozzles/m	Spray form
Case 1	0	0.8	Upwards spray
Case 2	0	1.0	Upwards spray
Case 3	0	1.2	Upwards spray
Case 4	0.2	0.8	Upwards spray
Case 5	0.2	1.0	Upwards spray
Case 6	0.2	1.2	Upwards spray
Case 7	0.2	0.8	Downwards spray
Case 8	0.2	1.0	Downwards spray
Case 9	0.2	1.2	Downwards spray
Case 10	0.4	0.8	Downwards spray
Case 11	0.4	1.0	Downwards spray
Case 12	0.4	1.2	Downwards spray

2.3 Spray-flow-evaporation coupling mechanism

The cooling effect of spray cooling is determined by the synergistic action of droplet dynamics, gas flow transport, and evaporation mass transfer. As listed in Table 6, in the spray stage, the size, initial velocity, and spatial distribution of the droplets produced by the nozzle are affected by the spray direction (upward/downward). Airflow stage: Natural convection or forced ventilation (such as fans) within the greenhouse alters the droplet trajectory and retention time. Evaporation stage: The enthalpy difference between the droplet surface and the air drives evaporation, absorbing sensible heat (cooling).

Table 6 Coupling effect of spray direction and airflow

Direction of spray	Droplet retention time	Interaction with airflow	Evaporation efficiency
Upwards spray	Longer (against gravity)	Susceptible to enhanced upward air currents	High (possibly unevenly distributed)
Downwards spray	Short (gravity acceleration)	Opposition of natural convection	Low (uniform)

2.4 Field experiment

2.4.1 Measurement and data collection system

RS-485 temperature and humidity sensors (Jianda Renko, RS-GZWS-N01-2-200 000, China, ±0.3°C, ±2% RH) were arranged in the east-west section of the greenhouse. The locations of the test points in the greenhouse are shown in Figure 4. The sensors recorded data once every minute, and all temperature and humidity data were processed equally.

2.4.2 Tomato cultivation experiment

The experiment was conducted from March to July 2023 in a double-layer spraying greenhouse and a single-layer multispan greenhouse of the same size at the Baima Base of Nanjing Agricultural University using the tomato cultivar ‘Qianxi’. An appropriate amount of full and uniform tomato seeds was selected and soaked in 55°C warm water for 10-20 min, stirring continuously during this process for seed sterilization. After naturally cooling to room temperature, the seeds were soaked for

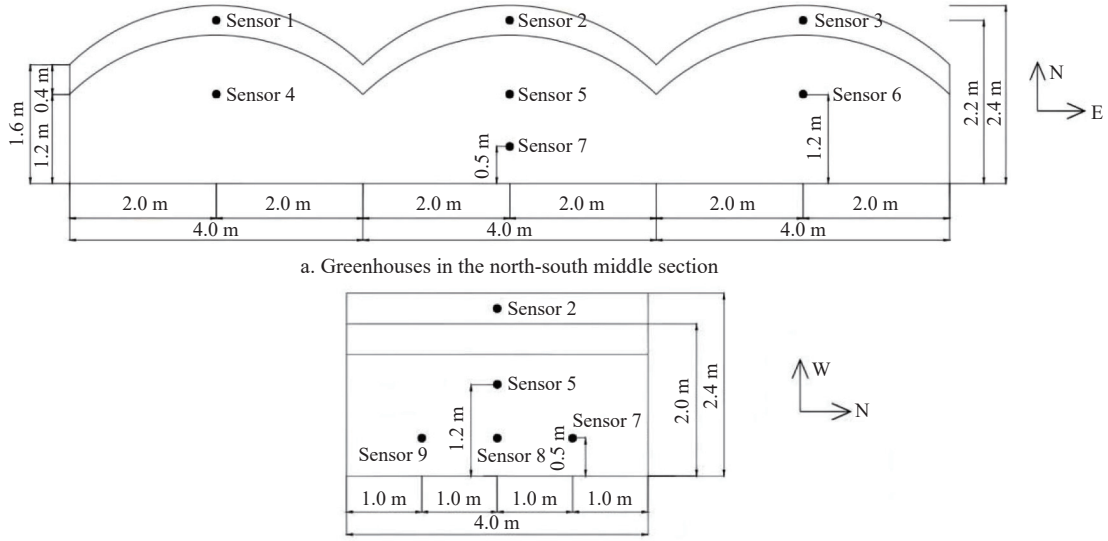

a. Greenhouses in the north-south middle section

b. Greenhouses in the middle span in the east-west direction of the middle section

Note: a: Greenhouses in the north–south middle section; and b: Greenhouses in the middle span in the east–west direction of the middle section.

Figure 4 Diagram of sensor distribution

another 2-4 h. Then, the seeds were wrapped in wet gauze, placed in an open plastic bag, and germinated in a constant temperature chamber at 28°C for 20-24 h. After germination, uniform seeds were planted in 32-hole seedling trays. When the tomato seedlings grew to a height of 20-25 cm with 5-6 true leaves, well-grown and uniform tomato plants were selected for transplanting into the greenhouse. The tomato plants were planted on March 16, with a spacing of 30 cm. The water and fertilizer management involved irrigating with nutrient solution (using *A* and *B* fertilizers in combination). From the seedling stage to the fruiting stage, the nutrient solution (Electrical Conductivity (EC) values from 1.8 to 2.0 mS/cm) was applied every 3-5 d, and from the fruiting stage to the harvesting period, the nutrient solution (EC value from 2.2 to 2.8 mS/cm) was applied based on weather conditions to meet the normal growth needs of the tomatoes. On days 20, 40, and 60 after tomato planting, three uniform tomato plants were randomly selected from the double-layer spraying greenhouse and the single-layer multispan greenhouse to measure their growth and photosynthetic parameters. Tomato yield and quality indicators were measured during the harvesting period, which started on June 15 and ended on July 1.

1) Plant growth indicators: Plant height was measured using a tape measure from the point of stem-root junction to the highest growth point. The thickness of the base of the plant stem was measured using a Vernier caliper, and the obtained value represents the stem diameter. The number of leaves was counted visually. The relative chlorophyll content was determined using a Soil and Plant Analyzer Development (SPAD) meter.

2) Tomato photosynthesis: The net photosynthetic rate (Pn), transpiration rate (Tr), intercellular CO_2 concentration (Ci), and stomatal conductance (Gs) were measured using a Li-6400 portable photosynthesis system. Measurements were taken from 9:00 to 11:00 AM on sunny days.

3) Fruit yield and quality: The yield per tomato plant was determined using an electronic balance. The soluble solids of the fruit were measured using a handheld refractometer, and the average value was taken from three repetitions. The soluble sugar content was determined using the anthrone colorimetric method. The titratable acid content of the fruit was measured using the sodium hydroxide titration method. The vitamin C content was determined using the 2,6-dichlorophenolindophenol titration method.

3 Results

3.1 Simulation and verification of the CFD model for a double-layer spray greenhouse

3.1.1 Validation of CFD models

To validate the accuracy of the CFD model, a comparison was made between the measured temperature data and the simulated data at 15:00 on a typical sunny day on June 9, 2023, at the measurement points inside the greenhouse. The results are presented in Table 7. Measurement Points 1 to 3 represent the misting layer, with a height of 2.2 m; Points 4 to 6 represent the plant canopy layer, with a height of 1.2 m; and Points 7 to 9 represent the near-ground layer, with a height of 0.5 m. As shown in the table, the CFD simulation results exhibit the same pattern as the measured values, with the lowest temperature observed in the misting layer and the highest in the plant canopy layer. This is because the spray nozzles are located within the double-layer film, and the continuous vaporization and heat absorption of the water mist result in a decrease in temperature in the misting layer. As the water mist does not directly contact the air inside the greenhouse, it relies only on the inner layer of the film for heat exchange, causing the cooling rate at the plant canopy height to be slower than that in the misting layer. Except for measurement Point 1, where the simulated value is lower than the measured value, the temperatures at the other measurement points are all higher than the measured values. The absolute error between the CFD-simulated temperatures and the measured values ranges from 0.03°C to 1.49°C, with a maximum relative error of 4.06%, an average absolute error of 0.81°C, and an average relative error of 2.25%. The observed discrepancies between measured and simulated values primarily stem from model simplification assumptions, particularly the idealized boundary conditions adopted in the simulation. In contrast, real-world natural conditions exhibit inherent variability (e.g., temporal fluctuations in wind velocity or thermal gradients). These errors fall within a reasonable range, indicating that this model can serve as an effective tool for designing and optimizing the layout of greenhouse spray systems.

Table 7 Comparison of the simulated and measured temperatures at the measuring points

Measuring point	Simulated value/°C	Measured value/°C	Absolute error/°C	Relative error/%
1	34.13	34.60	0.47	1.36
2	34.57	34.10	0.47	1.38
3	33.61	32.30	1.31	4.06
4	39.85	39.10	0.75	1.92
5	39.27	38.90	0.37	0.95
6	40.03	40.00	0.03	0.08
7	38.02	37.00	1.02	2.76
8	38.79	37.30	1.49	3.99
9	38.70	37.30	1.40	3.75

3.1.2 Analysis of the simulation results of the greenhouse temperature distribution

Figure 5 shows a contour map of the 3D temperature field of the greenhouse under spray cooling. The spray nozzles are installed on the inner layer of the greenhouse film, and water mist is sprayed towards the top layer of the film. As shown in the figure, the temperature distribution of the top layer of the greenhouse film exhibits a mesh-like pattern, with an average temperature of 36.04°C. The highest temperature of the top film is 42.25°C, which is distributed in areas where there are no atomized water droplets. The primary way for the greenhouse to absorb heat is through solar radiation, where sunlight strikes the plastic film, converts it into heat energy, and elevates the film temperature. When the coolant (water) is sprayed onto the surface of the top film by the nozzles, the water mist rapidly evaporates, absorbing heat from the film surface. Moreover, as spraying continues, a water film forms on the film, causing convective heat transfer, which further reduces the surface temperature of the film. Since the spray nozzles have a certain range, areas of the film without atomized water droplets tend to have relatively higher temperatures, resulting in the mesh-like temperature distribution observed on the top film. Analyzing the overall temperature distribution of the greenhouse in terms of height, it is evident that the upper layer (misting layer) has a lower temperature, while the lower layer has a higher temperature. The average temperature of the greenhouse misting layer is 33.37°C, while the average temperature of the lower layer is 37.65°C, with a difference of 4.28°C. This demonstrates a clear temperature stratification within the greenhouse.

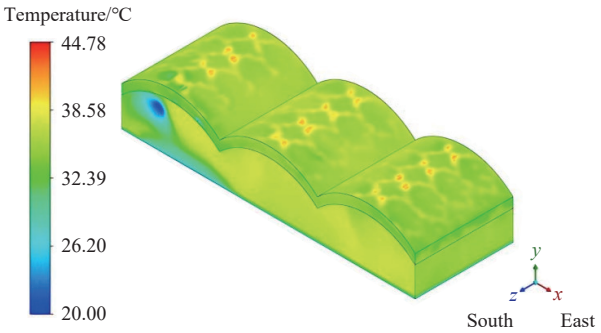

Figure 5 Temperature cloud of the greenhouse temperature field

To further analyze the temperature distribution in the greenhouse, the temperatures across the horizontal (*Z*-axis), longitudinal (*X*-axis), and horizontal (*Y*-axis) cross-sections are examined. Figure 6 shows the temperature contour map in the *Z*=2 m cross-section of the greenhouse. *Z*=2 m corresponds to the central region of the greenhouse. The coordinate system indicates that the *X*-axis points to the east, and the *Y*-axis represents the vertical direction. The temperature range is from 20.00°C (dark blue) to 44.78°C (dark red), with the color bar on the left providing a quantitative reference for temperature values. As shown in Figure 6, the temperature distribution in the misting layer of this cross-section is more uniform than that inside the greenhouse. Specifically, the temperature range in the misting layer is 25.53°C to 40.66°C, with an average temperature of 33.89°C, while the temperature range inside the greenhouse is 22.22°C to 40.68°C, with an average temperature of 38.37°C. Analysis of the internal temperature of the greenhouse reveals that the temperature at the top of the inner arch is higher, and as the height decreases, the temperature of the greenhouse continuously decreases, reaching its lowest point at ground level. Additionally, heat accumulation is observed in some areas beneath the inner arch. This is attributed to the double-layer film structure, which makes it difficult for heat entering the greenhouse to escape, increasing in temperature inside the greenhouse. As the hot air rises, it accumulates beneath the inner arch. As the nozzles spray, a water film forms on the inner film, exchanging heat with the air inside the greenhouse. Cold air sinks, causing the temperature near the ground to continuously decrease. In the east-west direction, the average temperature in the middle span of the greenhouse is lower than that in the west and east spans. The main reason is that the unevaporated water mist forms droplets that converge at the connection of the inner arches, resulting in greater cooling effects in the middle span and thus lower temperatures.

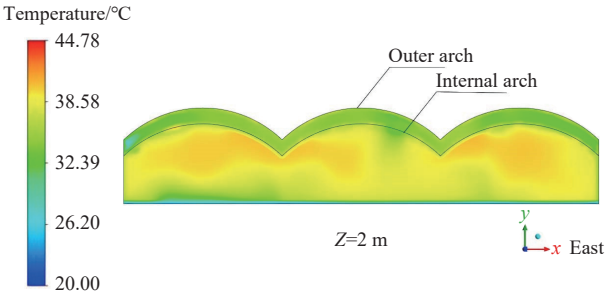

Figure 6 Temperature cloud in the greenhouse *Z*=2 m cross-section

Figure 7 presents the temperature contour maps of cross-sections located 2 m, 6 m, and 10 m from the west side of the film along the positive *X*-axis direction of the greenhouse. The coordinate system shows that the *X*-axis extends in the east-west direction, and the *Y*-axis represents the vertical direction. In the *X*=2 m section, there are obvious low-temperature areas (blue-green, 20.00°C-26.20°C) at the bottom and edges, while the middle and upper parts are in the higher-temperature range (yellow-orange, 32.39°C-38.58°C). In the *X*=6 m section, the temperature is mainly distributed in the yellow-orange range (32.39°C-38.58°C), with high-temperature areas (orange) concentrated at the top, and relatively uniform temperature distribution in the middle and upper parts. Similar to the *X*=6 m section, the *X*=10 m section has a temperature mainly in the yellow-orange range (32.39°C-38.58°C), with high-temperature areas concentrated at the top and relatively uniform temperature distribution in the middle and upper parts. As seen from the figure, the temperature distributions of all three cross-sections exhibit a trend of being lower at the top and bottom and higher in the middle, with heat accumulation occurring at top of the inner arch. The average temperature of *X*=2 m cross-section is lower than that of the *X*=6 m and *X*=10 m cross-sections, with average temperatures of 33.25°C, 37.83°C and 37.77°C, respectively.

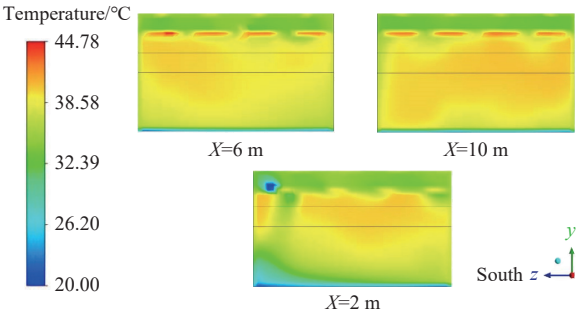

Figure 7 Temperature cloud in the *X*-axis section of the greenhouse

Figure 8 presents the temperature contour maps of the greenhouse cross-sections at heights of 0.5 m (*Y*=0.5 m, near-ground layer) and 1.2 m (*Y*=1.2 m, mid-upper layer) along the positive *Y*-axis (height direction). For the *Y*=0.5 m cross-section (near-ground layer), the lowest temperature is recorded at 26.17°C. This relatively low-temperature area may be influenced by factors such as the better heat exchange with the external environment on the west side or the more effective cooling effect of the double-layer spray system in this region. The highest temperature in this cross-section reaches 39.97°C, and the average temperature is 37.78°C. The presence of temperature differences indicates that although the near-ground layer is relatively close to the ground (which can have a certain thermal regulation effect), it is still affected by factors like solar radiation and uneven spray cooling. For the *Y*=1.2 m cross-section (mid-upper layer), the temperature ranges from 22.01°C to 40.36°C, with an average temperature of 38.67°C. The wider temperature range in this cross-section reflects the more complex heat transfer processes in the mid-upper layer of the greenhouse. The lower temperature values may be the result of the direct cooling effect of the double-layer spray system, where water mist evaporates and absorbs heat. However, the higher temperature values suggest that there are still areas where heat accumulation occurs.

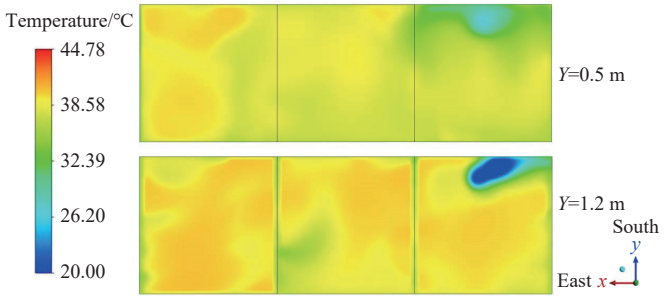

Figure 8 Temperature cloud in the *Y*-axis section of the greenhouse

Overall, the temperature near the top of the greenhouse arch is relatively high due to the continuous absorption of solar radiation by the inner arch film, which suspends hot air near the arch. Even though there is a misting layer for heat exchange between the inner arch film and the air inside the greenhouse, the lack of vents to expel the hot air accumulated at the top of the arch leads to heat accumulation, resulting in a higher temperature near the top of the arch. This explains the increasing trend of the temperature inside the greenhouse as the height increases.

3.2 Indoor temperature distribution of greenhouses under different nozzle layout conditions

3.2.1 Temperature analysis of greenhouse cross-sections under different working conditions

Figure 9 illustrates the temperature contour maps of the greenhouse's *Z*=2 m cross-section across 12 distinct working conditions, offering profound insights into thermal dynamics under varying spray configurations. As shown in the figure, the overall temperature distribution of the greenhouse is characterized by east–west symmetry, with higher temperatures in the eastern and western spans and lower temperatures in the middle span. When the upward spraying mode (Cases 1 to 6) is employed, the internal temperature distribution demonstrates a higher degree of uniformity. The upward-directed spray mist interacts with the air column, promoting extensive mixing. This mixing process effectively diffuses thermal energy across different regions of the greenhouse, minimizing the formation of extreme temperature differences. As a result, the temperature gradient across the *Z*=2 m cross-section is gentle, creating a more stable thermal environment that could be beneficial for crops sensitive to temperature fluctuations. In contrast, the adoption of downward spraying (Cases 7 to 12) induces a marked temperature stratification within the greenhouse. The spray mist, moving downward under gravity, concentrates its cooling effect in the lower regions near the ground. This causes the temperature near the ground to drop significantly, forming a cooler zone. However, the hot air accumulated at the top of the inner arch fails to be effectively dissipated. Without sufficient ventilation or counteracting cooling measures, this hot air lingers, leading to higher temperatures at the arch top. In Cases 10 to 12, this heat accumulation becomes particularly pronounced, with visible hotspots at the arch top. These hotspots indicate a severe imbalance in thermal management, where the downward spray fails to address the upper-layer heat, potentially endangering crops growing in the upper canopy or near the arch structure. The ranking of average internal temperatures, from highest to lowest—Case 5>Case 4>Case 6>Case 1>Case 2>Case 3>Case 12>Case 11>Case 10>Case 9>Case 8>Case 7—clearly demonstrates the superiority of downward spraying in cooling performance. Downward spraying, by directly targeting the lower regions where crops are predominantly located, can more effectively reduce the overall internal temperature, creating a more favorable environment for plant growth.

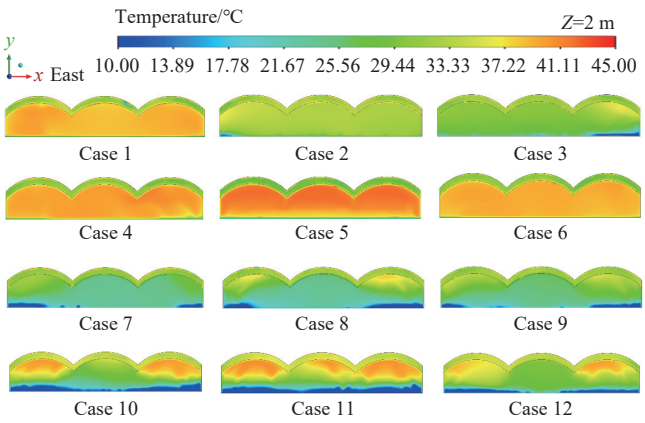

Figure 9 Temperature cloud in the *Z*=2 m section of the greenhouse under different schemes

3.2.2 Temperature analysis of greenhouse longitudinal sections under different working conditions

Figure 10 depicts the temperature contour map of the greenhouse's *X*=6 m cross-section under different scenarios. As shown in the figure, when the nozzles spray upwards (Cases 1 to 6),

there is a significant temperature stratification along the height of the greenhouse in this cross-section, which is characterized by lower temperatures in the spray layer and higher temperatures inside the greenhouse. When the nozzles spray downwards (Cases 7 to 12), there is a clear temperature gradient along the *Y*-axis (height direction), with the indoor temperature increasing as the height increases. Except for Case 10, the temperature distribution along the *Z*-axis (horizontal direction) in the greenhouse under other working conditions is highly uniform.

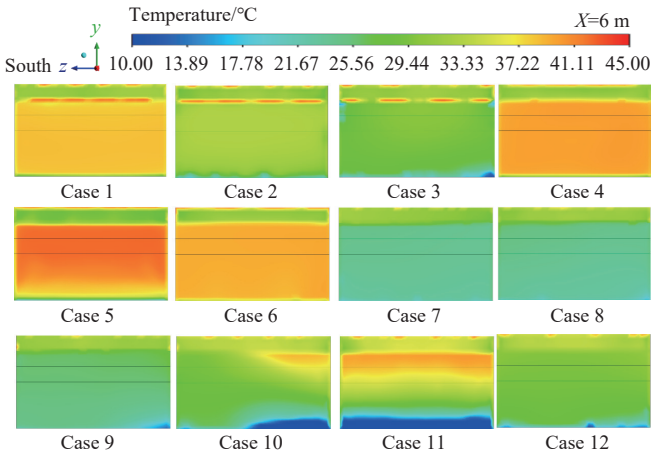

Figure 10 Temperature cloud in the *X*=6 m section of the greenhouse under different schemes

According to the temperature contour maps of Cases 1 to 12, regardless of the spraying method, the average air temperature inside the greenhouse gradually increases as the vertical distance between the nozzle and the top of the inner arch increases. Comparing the temperature contour maps of Cases 4 to 6 with those of Cases 7 to 9, it is found that the average indoor temperature of the downwards spraying method is lower than that of the upwards spraying method. The highest average temperature inside the greenhouse in Case 5 is 40.72°C, while the lowest average temperature in Case 7 is 23.76°C.

The temperature contour map results of Cases 1 to 6 show that when spraying upwards, the nozzle spacing has no obvious effect on the temperature in this cross-section. However, the results of Cases 7 to 12 show that when spraying downwards, the average indoor air temperature increases as the nozzle spacing increases.

3.2.3 Temperature analysis of greenhouse horizontal sections under different working conditions

Figure 11 depicts the temperature contour map of the greenhouse's *Y*=1.2 m cross-section under different scenarios. As shown in the figure, the temperature distribution in the *Y*=1.2 m cross-section is relatively uniform in Cases 1 to 9, while the uniformity of the temperature distribution in Cases 10 to 12 is poorer. Among them, Case 7 has the lowest average temperature in the *Y*=1.2 m cross-section of the greenhouse, which is 26.23°C. The order of the average temperatures from low to high in the other scenarios is Case 8<Case 9<Case 3<Case 12<Case 2<Case 10<Case 11<Case 1<Case 6<Case 4<Case 5. The scenarios with average cross-sectional temperatures above 35°C are Case 1, Case 4, Case 5, Case 6, and Case 11. The scenarios with average temperatures less than 30°C include Case 7, Case 8, and Case 9, all of which use a downwards spraying method with nozzles placed 0.2 m above the top of the inner arch. The temperature distributions in the height cross-sections of Cases 7 to 12 are similar, with higher temperatures on the east and west sides and lower temperatures in the middle. Compared to Cases 7 to 9, Cases 10 to 12 have more heat accumulation and higher temperatures across the east–west span of the greenhouse. The results indicate that when using the same spraying method, the closer the nozzle is to the top of the inner arch, the better the cooling effect. Comparing the results of Cases 1 to 6 with those of Cases 7 to 12 suggests that downwards spraying by the nozzles is more effective at cooling than upwards spraying.

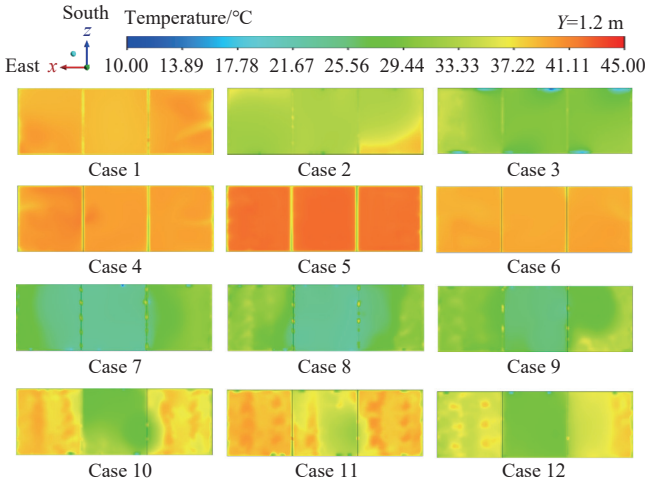

Figure 11 Temperature cloud in the *Y*=1.2 m section of the greenhouse under different schemes

3.3 Study on the indoor microclimate of a double-layer spray greenhouse

3.3.1 Study on the indoor microclimate in the spring in a double-layer spray greenhouse

Figure 12 shows the changes in temperature, relative humidity, and illumination inside and outside the greenhouse from March 23rd to March 25th, 2023. On March 23rd, it was rainy, March 24th was cloudy, and March 25th was sunny. As shown in Figure 12a, the average temperatures inside the double-layer spray greenhouse, the single-layer multispan greenhouse, and outside were 11.26°C, 10.08°C, and 9.10°C, respectively. During this period, the lowest outside temperature was 0.80°C (at 23:30 on March 24th). At this time, the indoor temperature of the single-layer multispan greenhouse was 1.70°C, and the indoor temperature of the double-layer spray greenhouse was 2.60°C. As shown in Figure 12b, the average relative humidities inside the double-layer spray greenhouse, the single-layer multispan greenhouse, and outside were 81.46%, 86.31%, and 88.16%, respectively. The changes in relative humidity inside the double-layer spray greenhouse and the single-layer multispan greenhouse were consistent with those outside, but the indoor relative humidity in the double-layer spray greenhouse was lower than that in the single-layer multispan greenhouse, and the outside relative humidity was the highest. Figure 12c shows that the average illumination levels inside the double-layer spray greenhouse, the single-layer multispan greenhouse, and outside were 2.53 klx, 2.76 klx, and 3.61 klx, respectively. On the rainy day of March 23rd, the average illumination of the three regions was 1.43 klx, 1.65 klx, and 1.94 klx. On the cloudy day of March 24th, the average illumination levels were 2.45 klx, 2.61 klx, and 3.43 klx, respectively. On the sunny day of March 25th, the average illumination levels were 3.72 klx, 4.01 klx, and 5.46 klx, respectively.

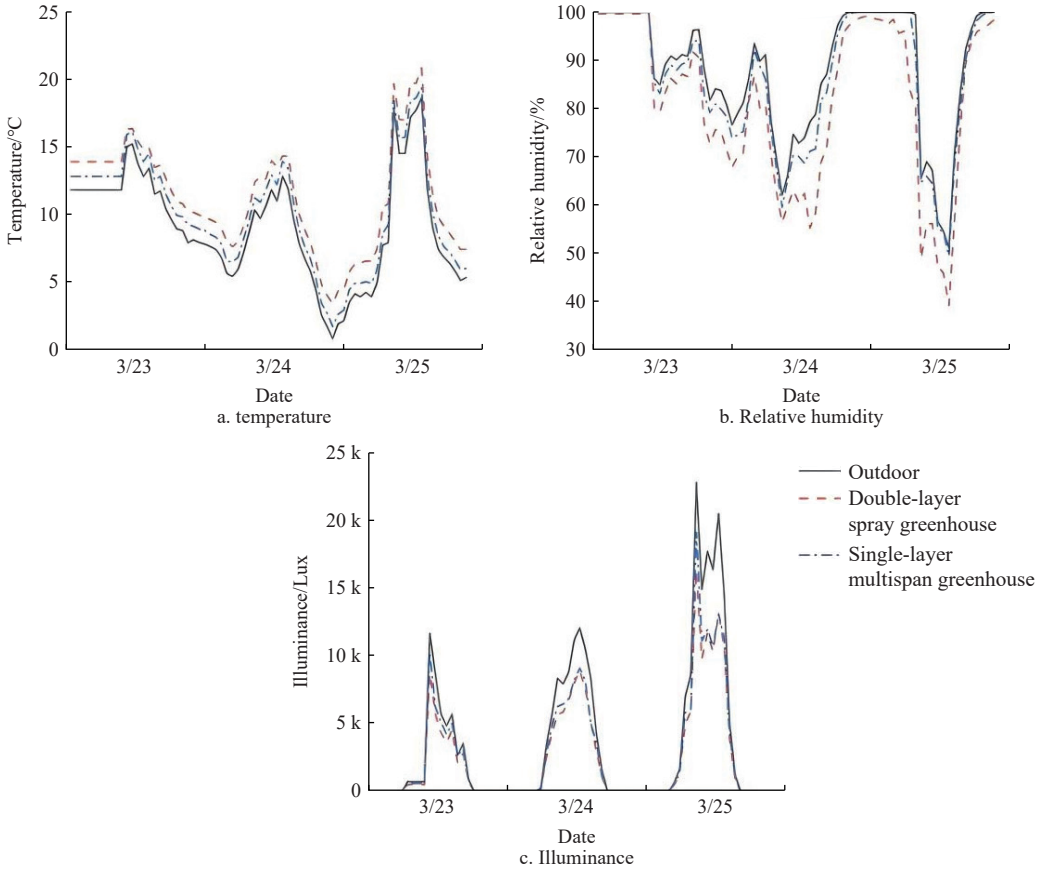

Note: a: temperature; b: relative humidity; and c: illuminance.

Figure 12 Changes in temperature, relative humidity, and illuminance inside and outside the greenhouse in spring 2023

3.3.2 Study on the indoor microclimate in summer in a double-layer spray greenhouse

The double-layer spray greenhouse was sprayed under sunny weather conditions from June 1 to July 1, 2023. The operating hours ranged from 09:00 to 17:00 daily, with a water supply pressure of 6 MPa. Each spraying session lasted for 15 min, followed by a 15-min pause, and this cycle was repeated. The vents on the north-west side of both greenhouses were open during this period (vent height 1.6 m). Figure 13 shows the changes in the inside and outside temperatures, relative humidity, and illumination intensity under typical sunny conditions from June 20 to June 22, 2023. The spray system in the double-layer spray greenhouse used nozzles with a diameter of 0.30 mm. The nozzle layout consisted of 120° double nozzles spaced 0.8 m apart, placed 0.2 m below the inner vault and sprayed downwards. As shown in Figure 13a, the average temperatures inside the double-layer spray greenhouse, single-layer multispan greenhouse, and outside from 09:00 to 17:00 were 37.65°C, 39.79°C, and 35.24°C, respectively. During this period, the highest temperature inside the double-layer spray greenhouse was 45.53°C (at 13:30 on June 20); at this time, the outside temperature was 45.23°C, while the temperature inside the single-layer multispan greenhouse was 50.00°C, 4.47°C higher than that inside the spray greenhouse. As depicted in Figure 13b, the relative humidity changes in the double-layer spray greenhouse, single-layer multispan greenhouse, and outside were consistent. Specifically, the indoor relative humidity in the double-layer spray greenhouse during the day was significantly greater than that in the single-layer multispan greenhouse and outside. The average relative humidity from 09:00 to 17:00 for these three environments was 60.61%, 55.51%, and 51.96%, respectively. Figure 13c illustrates the changes in illumination intensity inside and outside the greenhouse. During the test period from 09:00 to 17:00, the indoor illumination intensity in the double-layer spray greenhouse was lower than that in the single-layer multispan greenhouse, but both indoor illumination intensities were significantly lower than the outside illumination intensity. The average illumination intensities in the double-layer spray greenhouse, single-layer multispan greenhouse, and outside were 14.45 klx, 16.99 klx, and 25.48 klx, respectively. The highest outside illumination intensity was 114.97 klx, the highest indoor illumination intensity in the double-layer spray greenhouse was 65.53 klx, and the highest indoor illumination intensity in the single-layer multispan greenhouse was 80.01 klx. The highest indoor illumination intensity in the double-layer spray greenhouse was 14.48 klx lower than that in the single-layer multispan greenhouse and 49.44 klx lower than that outside.

3.4 Study on the effect of tomato cultivation in a double-layer spray greenhouse

3.4.1 Analysis of tomato growth in a double-layer spray greenhouse

Figure 14 depicts the growth indicators of tomato plants in different types of greenhouses. As shown in the figure, the plant height, stem diameter, and leaf chlorophyll content (SPAD) of the tomato plants in the double-layer spray greenhouse were greater than those in the single-layer multispan greenhouse on the 20th, 40th, and 60th days after planting (March 16, 2023). There was no significant difference in tomato plant height between the two types of greenhouses, but there was a significant difference in stem diameter. The tomato plant height in the double-layer spray greenhouse was 0.94-5.08 cm greater, and the stem diameter was 0.76-1.52 cm greater than that in the single-layer multispan

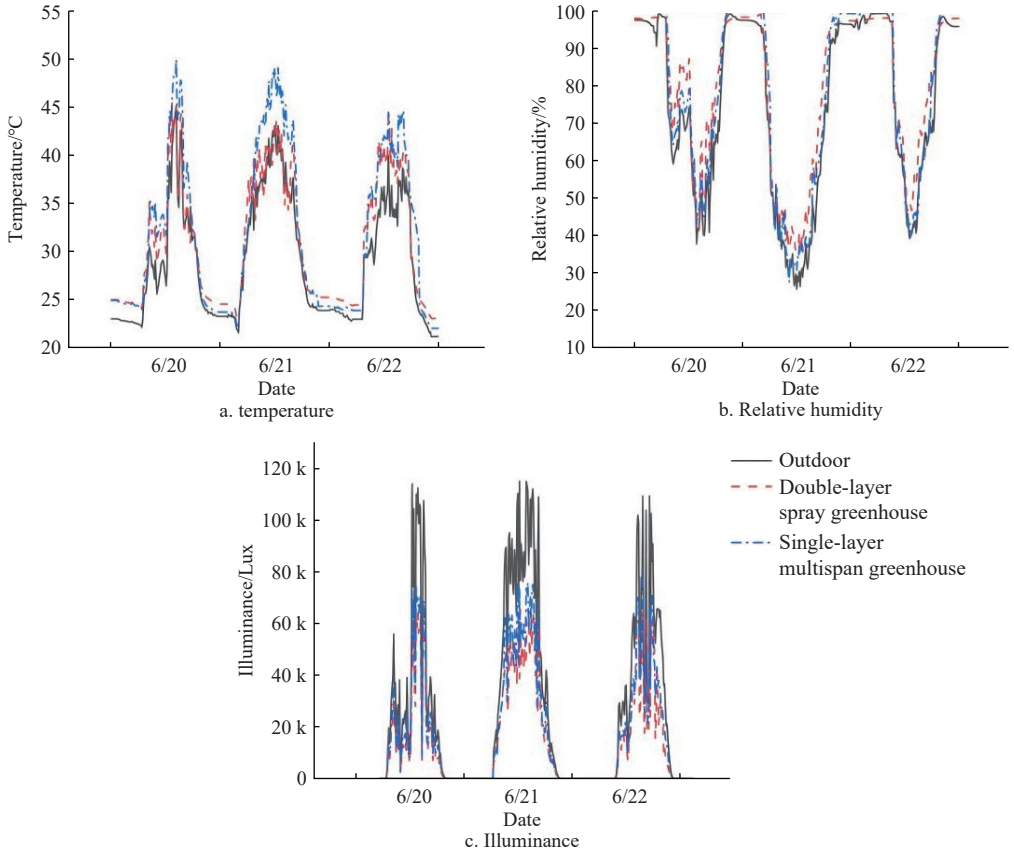

Note: a: temperature; b: relative humidity; c: illuminance

Figure 13 Changes in temperature, relative humidity, and illuminance inside and outside the greenhouse in summer 2023

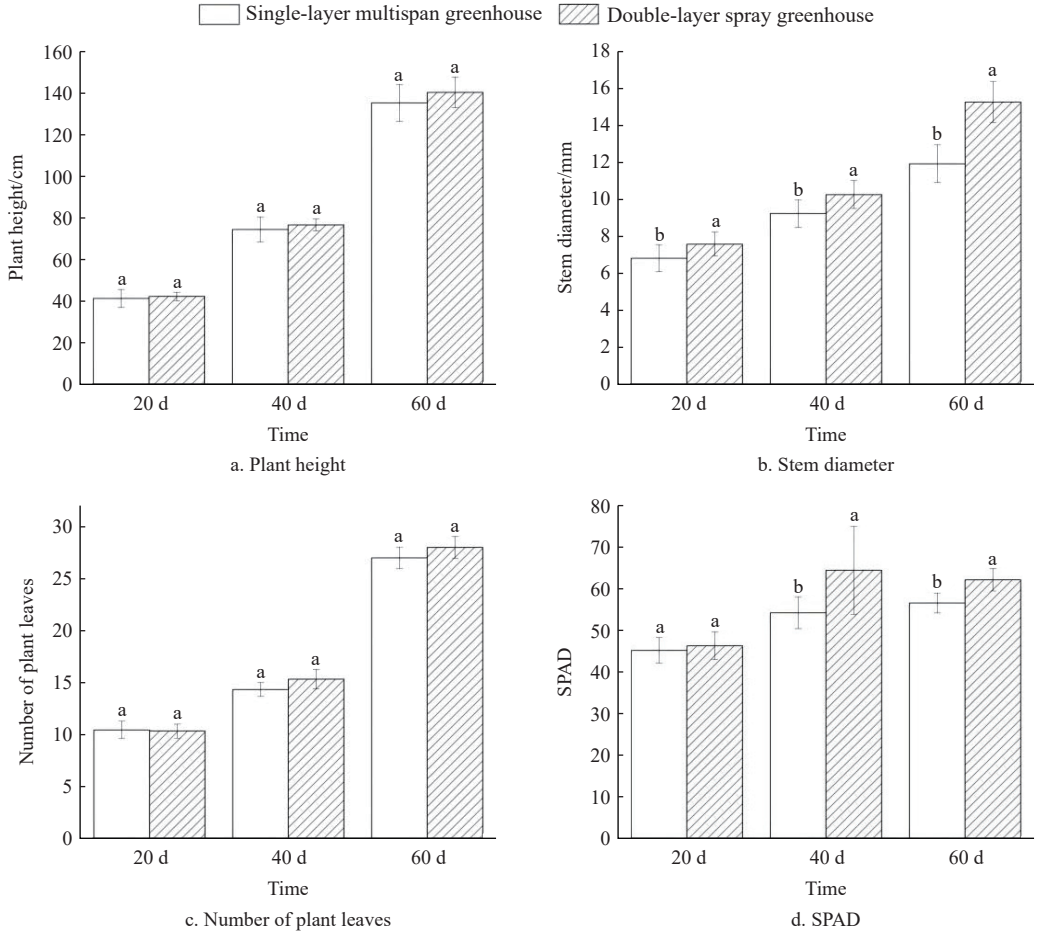

Note: a: plant height; b: stem diameter; c: number of plant leaves; and d: SPAD

Figure 14 Growth indices of tomato plants in different greenhouses

greenhouse. As shown in Figure 14c, on the 20th day after planting, the number of leaves on plants in the single-layer multispan greenhouse was similar to that in the double-layer spray greenhouse. However, on the 40th and 60th days after planting, the double-layer spray greenhouse had more tomato leaves, but the difference was not significant. Figure 14d shows that on the 40th day after planting, the SPAD of tomato leaves in the double-layer spray greenhouse was significantly greater than that in the single-layer multispan greenhouse, being 10.23 greater. In comparison, the growth conditions of tomatoes in the double-layer spray greenhouse were better.

3.4.2 Analysis of tomato photosynthesis in a double-layer spray greenhouse

Figure 15 shows the photosynthetic parameters of tomato plants in different types of greenhouses. As shown in Figure 15a, on the 20th day after planting, the net photosynthetic rate (Pn) of the tomatoes in the double-layer spray greenhouse was significantly greater than that in the single-layer multispan greenhouse. At this time, the Pn of the tomatoes in the double-layer multispan greenhouse was 24.22 μmol/(m^2·s), while the Pn of the tomatoes in the single-layer multispan greenhouse was 16.10 μmol/(m^2·s). On the 40th day after planting, the Pn of the tomatoes in the double-layer spray greenhouse was 0.9 μmol/(m^2·s) lower than that in the single-layer multispan greenhouse, but the difference was not significant. On the 60th day after planting, the Pn of the tomatoes in the double-layer spray greenhouse was 5.23% greater than that in the single-layer multispan greenhouse. As depicted in Figure 15b, on the 20th and 40th days after planting, the stomatal conductance (Gs) of the tomatoes in the double-layer spray greenhouse was significantly greater than that in the single-layer multispan greenhouse. On the 60th day after planting, the Gs of the tomatoes in the double-layer spray greenhouse was greater than that in the single-layer multispan greenhouse, but the difference was not significant. Figure 15c indicates that on the 20th, 40th, and 60th days after planting, the intercellular CO_2 concentration (Ci) of tomatoes in the double-layer spray greenhouse was greater than that in the single-layer multispan greenhouse. On the 20th and 60th days after planting, the difference in Ci between the two types of greenhouses was not significant. According to Figure 15d, the transpiration rate (Tr) of tomatoes in the double-layer spray greenhouse was significantly greater than that in the single-layer multispan greenhouse on the 40th day after planting, at 0.35 mmol/(m^2·s). This suggests that the utilization efficiency of light energy in tomato plants in a double-layer spray greenhouse is superior to that in a single-layer multispan greenhouse.

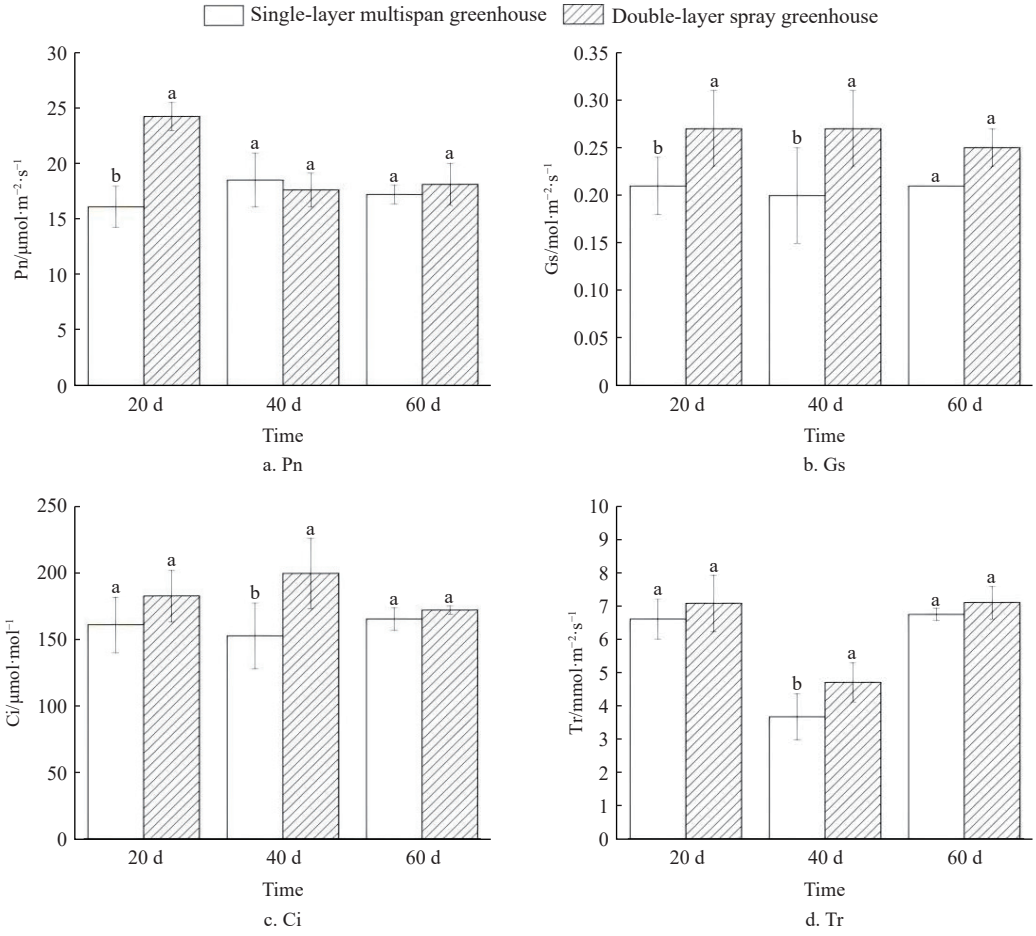

Note: a: Pn; b: Gs; c: Ci; and d: Tr.

Figure 15 Photosynthetic parameters of tomatoes in different greenhouses

3.4.3 Yield and fruit quality analysis of tomato plants in a double-layer spray greenhouse

As listed in Table 8, the contents of soluble solids, vitamin C, and soluble sugar in tomato fruits in the double-layer spray greenhouse were greater than those in the single-layer multispan greenhouse, with increases of 4.78%, 9.09%, 13.35%, and 17.69%, respectively. The differences in soluble solids content and vitamin C content between the two types of greenhouses were not significant. The titratable acid content of tomato fruits in the single-layer multispan greenhouse was 0.12% greater than that in the double-layer spray greenhouse. In terms of yield per plant, the tomato yield in the double-layer spray greenhouse was 7.52%

greater than that in the single-layer multispan greenhouse. Although tomatoes in the double-layer spray greenhouse did not show a significant advantage in yield or quality, they began to change color on June 5, 2023, while those in the single-layer multispan greenhouse began to change color on June 9. This earlier harvest in the double-layer spray greenhouse was more advantageous.

Table 8 Fruit yield per plant and quality indicators of tomatoes from different greenhouses

Greenhouse types	Soluble protein/%	Vc/ mg·g^{-1}	Soluble sugar/%	Titratable acid/%	Yield per plant/g·plant^{-1}
Single-layer multispan greenhouse	2.93±0.01^{a}	0.22±0.01^{a}	13.48±0.01^{b}	3.06±0.00^{a}	576.00±297.88^{a}
Double-layer spray greenhouse	3.07±0.01^{a}	0.24±0.01^{a}	15.28±0.03^{a}	2.94±0.00^{a}	619.33±190.27^{a}

Note: Different lowercase letters indicate significant differences between different treatments (p<0.05).

3.5 Study on the cost and energy consumption of the spray system in double-layer spray greenhouse

Studying the costs and energy consumption of cooling systems can promote the rational utilization of resources and help further optimize spray cooling systems. McCartney[13] investigated the energy consumption of a pad-fan cooling system in a greenhouse with an area of 13.7 m×32 m. This section estimates the costs and energy consumption of a spray cooling system in a greenhouse in the same area. Table 9 presents the cost estimates for the spray system and the pad-fan system. As shown in the table, the spray system mainly comprises a spray host, spray pipes, and nozzles, while the pad-fan system consists of a pad, fans, a water tank, and a water pump. The total cost of the spray system is 785 RMB lower than that of the pad-fan system.

Table 9 Cost estimates for different cooling systems

Cooling system	Device	Number	Price/ RMB	Total cost/¥
Spray system	9.52 mm polyethylene pipe	150 m	255	4355
	0.30 mm diameter nozzle	200	600	
	Spray engine (including 10 MPa booster pump, 100 mm filter level filter, 16 L water tank, and automatic switch)	1	3500	
Fan-pan system	Aluminum alloy wet curtain (height 1.8 m, width 0.6 m, and thickness 0.15 m)	20	2300	5120
	380 V negative pressure fan	4	1600	
	800 L water tank	1	300	
	380 V horizontal centrifugal water pump	1	920	

As listed in Table 10, based on the measured data from the experimental greenhouse in 2023 (with an average daily operation of 8 h in summer) and considering the typical growth period of tomatoes (90–110 d), a dynamic cost analysis was conducted to compare the resource utilization efficiency of the two systems. In Nanjing, the agricultural electricity price is 0.51 RMB/kW·h, and the agricultural water price is 3.82 RMB/t. The spray system consumed an average of 11.2 kW·h of electricity per day, costing 5.71 RMB/d, while the pad-fan system consumed 39.2 kW·h/d, amounting to 19.99 RMB/d. In terms of water consumption, the spray system used 1.92 t/d (7.33 RMB/d), whereas the pad-fan system required 3.79 t/d (14.47 RMB/d). Taking the tomato growth cycle (100 d, with 60 d requiring cooling during high-temperature periods), the total lifecycle cost of the spray system (794.4 RMB) was 1273.2 RMB lower than that of the pad-fan system (2067.6 RMB), representing a 61.57% reduction. This significant cost savings primarily stems from lower energy consumption (reduced electricity usage) and more efficient water utilization (water savings).

Table 10 Energy consumption estimation of different cooling systems

Cooling system	Daily electricity consumption/ kW·h·d^{-1}	Daily water consumption/ t·d^{-1}	Electric charge/ RMB·d^{-1}	Water cost/ RMB·d^{-1}
Spray system	11.2	1.92	5.71	7.33
Fan-pan system	39.2	3.79	19.99	14.47

4 Discussion

CFD can accurately simulate the temperature distribution of a spray system in a greenhouse, greatly reducing the time, labor, material, and financial resources required for experiments[8,14]. In this study, CFD technology was used to simulate the temperature field inside a double-layer spray greenhouse under spray cooling in summer. The temperature in the arch region inside the greenhouse was relatively high, and as the height decreased, the air temperature inside the greenhouse continuously decreased, with the lowest temperature occurring at ground level. The nozzle placement height is an important factor affecting the droplet coverage area and significantly affects the heat transfer process[15]. When other conditions remain unchanged, as the nozzle placement height increases, the average temperature inside the greenhouse increases. The influence of the nozzle spacing on the cooling effect of the greenhouse is related to the nozzle spraying pattern. Only when the nozzles spray downwards does the average indoor air temperature increase with increasing nozzle spacing. In addition, spraying downwards has a better cooling effect than spraying upwards, consistent with the results of Wang et al.[16]. Since the spray system is installed inside the double-layer film, its cooling effect mainly relies on heat exchange between the inner layer of the greenhouse film and the internal environment. When the nozzles spray upwards, the fine droplets first contact the inner surface of the outer layer of the greenhouse film. As the nozzles continue to spray upwards, an internal mist layer gradually forms, and a water film forms on the inside of the outer layer of the greenhouse film, while the mist may accumulate on the surface of the inner layer of the greenhouse film, forming water droplets. When the nozzles spray downwards, the sprayed mist directly contacts the outer surface of the inner layer film, quickly forming a water film on its surface. In contrast, the heat transfer of the water film formed by downwards spraying is more continuous and stable on the inner layer of the greenhouse film. When the water film flows, it can carry away heat from the arch top inside the greenhouse, improving the efficiency of convective heat exchange.

The average indoor temperature in the double-layer spray greenhouse in spring was 1.18°C higher, the average light intensity was 0.23 kW/L lower, and the average relative humidity was 4.85% lower than that in the single-layer greenhouse. In summer, the average indoor temperature was 1.07°C lower, the average light intensity was 2.54 kL lower, and the average relative humidity was 1.54% higher than those in the single-layer greenhouse, verifying the insulating effect of the double-layer structure and the cooling effect of the spray system in summer. Temperature and light environment are key factors affecting tomato growth and fruit quality. As a crucial factor affecting dry matter production and distribution, it directly correlates with the fruit quality and yield of crops. Light is one of the essential energy sources for plants to carry

out photosynthesis and is also a crucial signal for plant growth. Light plays a significant role in plant morphogenesis, physiological metabolism, and biomass accumulation[17]. Moreover, photosynthesis is affected by temperature, and both low and high temperatures can reduce the photosynthetic rate of plants[18-20]. Tomatoes prefer warmth but are not heat tolerant, with an optimal growth temperature range of 15°C-25°C. When the growth environment is below 12°C, tomato crops may suffer from chilling injury; when the temperature is below 5°C, tomato growth stops; when the temperature is above 35°C, tomato flowering and fruiting occur; and when the temperature is above 40°C, tomato growth stops. The plant height, stem diameter, yield, fruit soluble solids content, vitamin C content, and soluble sugar content of the tomatoes in the double-layer spray greenhouse were all greater than those in the single-layer greenhouse. Compared with the pad-fan system, the spray system has lower costs, daily electricity consumption, and daily water consumption. Further optimization of greenhouse spray systems should be carried out to reduce energy consumption and promote sustainable horticultural production. In addition, in practice, the airflow disturbance within the double membrane structure may lead to uneven spray distribution and affect the cooling efficiency, so it is recommended to use rotating nozzles to optimize the coverage; at the same time, the long-term operation of the mineral deposition easily causes nozzle clogging, so it is recommended to use a self-cleaning filter or low-mineral water source to maintain system stability. This study provides a theoretical basis for the engineering design of greenhouse spray cooling systems by establishing a quantitative relationship between nozzle parameters and temperature field responses. Future work will further combine multi-objective optimization algorithms to systematically investigate the interaction among various parameters of the spray system and establish a more complete prediction model for spray cooling performance, with the aim of providing universal design guidance for spray systems in greenhouses of different structures.

5 Conclusions

To address the problems of high summer temperatures and low winter temperatures in plastic greenhouses in the middle and lower reaches of the Yangtze River, a double-layer spray greenhouse was designed in the early stage. This greenhouse utilizes a double-layer plastic film structure to enhance the insulation effect in winter and places a spray system composed of nozzles between the two layers of plastic film. During high-temperature seasons, the spray system is turned on, and the mist droplets are vaporized, thereby absorbing heat and reducing the temperature of the top of the greenhouse and ultimately reducing the temperature in the cultivation area. To further improve the cooling effect of the double-layer spray greenhouse in summer, this study used CFD to design the spray system and formed an optimal nozzle layout plan. At the same time, the effectiveness of the double-layer spray greenhouse was explored, and a comparative analysis of the inside and outside environmental factors of the two types of greenhouses under typical weather conditions in spring and summer was conducted using a single-layer multispan greenhouse as a control. Using ‘Qianxi’ tomatoes as the experimental material, the tomato growth indicators and fruit quality in the two greenhouses were measured. In addition, the cost and energy consumption of the spray system in the double-layer spray greenhouse were investigated, providing a reference for further improvement of the double-layer spray greenhouse and sustainable development of horticultural production. The main conclusions are as follows:

1) CFD technology was used to simulate the indoor temperature field during the summer spraying and cooling of the double-layer spray greenhouse. The measured environmental values in the greenhouse were used as the initial boundary conditions for the CFD simulation. By comparing the measured values and simulated values at the measurement points, it was verified that the maximum relative error was 4.06% and the average relative error was 2.25%, within a reasonable range, thus verifying the validity and accuracy of the model. The indoor temperature field of the double-layer spray greenhouse was analyzed, and it was found that the average temperature of the misting layer was significantly lower than the internal temperature of the greenhouse. At the same time, the temperature at the top of the greenhouse was relatively high, and as the height decreased, the air temperature inside the greenhouse continued to decrease, with the lowest temperature occurring at ground level.

2) The verified CFD model was used to simulate the temperature distribution in the greenhouse under different nozzle layout schemes. The simulation results showed that when other conditions remained unchanged, there was a positive correlation between the nozzle installation height and the indoor temperature. In addition, spraying the mist downwards from the nozzles had a better cooling effect than spraying it upwards. Among the 12 simulation schemes, Case 7 (with a nozzle spacing of 0.8 m, a nozzle installation height of 0.2 m from the top of the inner arch, and spraying the mist downwards) had the lowest average temperature inside the greenhouse, making it the optimal nozzle layout scheme.

3) Compared with that in the single-layer multispan greenhouse, the average indoor temperature in the double-layer spray greenhouse was 1.18°C higher in spring, with a lower average illumination intensity of 0.23 lux and a lower average relative humidity of 4.85%. In summer, the average indoor temperature was 2.14°C lower, with a lower average illumination intensity of 2.54 kL and a lower average relative humidity of 5.10%. The tomato growth (plant height and stem diameter), yield, and fruit quality (soluble solids content, vitamin C content, and soluble sugar content) in the double-layer spray greenhouse were better than those in the single-layer multispan greenhouse. The cost of the spray system, daily electricity consumption, and daily water consumption were lower than those of the wet curtain fan system.

Acknowledgements

This work was supported by the Open Project of Xinjiang Production & Construction Corps Key Laboratory of Protected Agriculture (Grant No. NJSS2024102), and the Science and Technology Plan Project of the First Division, Aral City (Grant No. 2022NY07) . The authors declare no conflict of interest.

[References]

[1] Tawalbeh M, Aljaghoub H, Alami A H, Olabi AG. Selection criteria of cooling technologies for sustainable greenhouses: A comprehensive review. Thermal Science and Engineering Progress, 2023; 38: 101666.

[2] Ghani S, Bakochristou F, ElBialy E M A A, Gamaledin S M A, Rashwan M M, Abdelhalim A M, et al. Design challenges of agricultural greenhouses in hot and arid environments - A review. Engineering in Agriculture, Environment and Food, 2019; 12(1): 48–70.

[3] Boulard T, Baille A. A simple greenhouse climate control model incorporating effects of ventilation and evaporative cooling. Agricultural and Forest Meteorology, 1993; 65(3): 145–157.

[4] Katsoulas N, Savvas D, Tsirogiannis I, Merkouris O, Kittas C. Response of an eggplant crop grown under Mediterranean summer conditions to greenhouse fog cooling. Scientia Horticulturae, 2009; 123(1): 90–98.

[5] Villarreal-Guerrero F, Flores-Velazquez J, Kacira M. Comparative performance of a greenhouse cooling strategy with natural ventilation and fogging under different outside climates. Acta Horticulturae, 2014; 1037: 57–64.

[6] Liu X L, Fu Y S, Yi L Y. Application of combined cooling system in summer production of agricultural greenhouses. Modern Agriculture, 2020; 41(3): 66–68. (in Chinese)

[7] Hamilton S W, De Peters E J, Mc Garve J A, Lathrop J, Mitloehner F M. Greenhouse gas, animal performance, and bacterial population structure responses to dietary monensin fed to dairy cows. Journal of Environmental Quality, 2010; 39(1): 106–114.

[8] Tamimi E, Kacira M, Choi C Y, Lingling An. Analysis of microclimate uniformity in a naturally vented greenhouse with a high-pressure fogging system. Transactions of the Asabe, 2013; 56(3): 1241–1254.

[9] Hu Y G, Chen Y K, Wei W Z, Hu Z Y, Li P P. Optimization design of spray cooling fan based on CFD simulation and field experiment for horticultural crops. Agriculture, 2021; 11(6): 566.

[10] Ghoulem M, El Moueddeb K, Nehdi E, Zhong F L, Calautit J. Analysis of passive downdraught evaporative cooling windcatcher for greenhouses in hot climatic conditions: Parametric study and impact of neighbouring structures. Biosystems Engineering, 2020; 197: 105–121.

[11] Xu J H, Bai W T, Wang J, Mu Z H, Sun W Z, Dong B D, et al. Study on the cooling effect of double-layer spray greenhouse. Agriculture, 2023; 13(7): 1442.

[12] Launder B E, Spalding D B. The numerical computation of turbulent flow. Computer Methodsin Applied Mechanics and Engineering, 1974; 3(2): 269–289.

[13] McCartney L, Lefsrud M G. Field trials of the natural ventilation augmented cooling (NVAC) greenhouse. Biosystems Engineering, 2018; 174: 159–172.

[14] Kim K, Giacomelii G A, Yoon J Y, Sase S, Son J E, Nam S W, et al. CFD Modeling to improve the design of a fog system for cooling greenhouses. Japan Agricultural Research Quarterly, 2007; 41(4): 283–290.

[15] Cheng W L, Liu Q N, Zhao R, Fan H L. Experimental investigation of parameters effect on heat transfer of spray cooling. Heat and Mass Transfer, 2010; 46: 911–921.

[16] Wang Y J, He F Y, Lv Z H, Yang W B, Wang Q. Experimental investigations on thermal performance of spray cooling double skin face in hot humid climate region. Energy and Buildings, 2022; 277: 112605.

[17] Dulai S, Molnar I, Molnar-Lang M. Changes of photosynthetic parameters in wheat/barley introgression lines during salt stress. Acta Biologica Szegediensis, 2011; 55(1): 73–75.

[18] Ashraf M, Harris P J C. Photosynthesis under stressful environments: An overview. Photosynthetica, 2023; 51(2): 163–190.

[19] Gerganova M, Popova A V, Stanoeva D, Velitchkova M. Tomato plants acclimate better to elevated temperature and high light than to treatment with each factor separately. Plant Physiology and Biochemistry, 2016; 104: 234–241.

[20] Verheul M J, Maessen H F R, Paponov M, Panosyan A, Kechasov D, Naseer M, et al. Artificial top-light is more efficient for tomato production than inter-light. Scientia Horticulturae, 2022; 291: 110537.